European Journal of Medicinal Chemistry 188 (2020) 112006

Contents lists available at ScienceDirect

European Journal of Medicinal Chemistry

journal homepage: http://www.elsevier.com/locate/ejmech

Research paper

Design, synthesis and biological evaluation of novel TRβ selective agonists sustained by ADME-toxicity analysis

Massimiliano Runfola [a, 1], Simona Sestito [a, 1], Lorenza Bellusci [b], Valeria La Pietra [c], Vincenzo Maria D'Amore [c], Marta Anna Kowalik [d], Grazia Chiellini [b, **], Sheraz Gul [e], Andrea Perra [d], Amedeo Columbano [d], Luciana Marinelli [c], Ettore Novellino [c], Simona Rapposelli [a, f, *]

[a] Department of Pharmacy, University of Pisa, Pisa, 56126, Italy
[b] Department of Pathology, University of Pisa, Pisa, 56126, Italy
[c] Department of Pharmacy, University of Naples Federico II, Italy
[d] Department of Biomedical Sciences, Unit of Oncology and Molecular Pathology, University of Cagliari, Cagliari, Italy
[e] Fraunhofer Institute for Molecular Biology & Applied Ecology – ScreeningPort, Hamburg, Germany
[f] Interdepartmental Research Centre for Biology and Pathology of Aging, University of Pisa, Pisa, Italy

ARTICLE INFO

Article history:
Received 24 September 2019
Received in revised form
11 December 2019
Accepted 20 December 2019
Available online 23 December 2019

Keywords:
Triiodothyronine
Thyronamine
TRβ selective agonist
Fatty-liver disorder
Liver regeneration

ABSTRACT

Although triiodothyronine (T3) induces several beneficial effects on lipid metabolism, its use is hampered by toxic side-effects, such as tachycardia, arrhythmia, heart failure, bone and muscle catabolism and mood disturbances. Since the α isoform of thyroid hormone receptors (TRs) is the main cause of T3-related harmful effects, several efforts have been made to develop selective agonists of the β isoform that could induce some beneficial effects (i.e. lowering triglyceride and cholesterol levels reducing obesity and improving metabolic syndrome), while overcoming most of the adverse T3-dependent side effects. Herein, we describe the drug discovery process sustained by ADME-Toxicity analysis that led us to identify novel agonists with selectivity for the isoform TRβ and an acceptable off-target and absorption, distribution metabolism, excretion and toxicity (ADME-Tox) profile. Within the small series of compounds synthesized, derivatives **1** and **3**, emerge from this analysis as "potentially safe" to be engaged in preclinical studies. In in vitro investigation proved that both compounds were able to reduce lipid accumulation in HepG2 and promote lipolysis with comparable effects to those elicited by T3, used as reference drug. Moreover, a preliminary in vivo study confirmed the apparent lack of toxicity, thus suggesting compounds **1** and **3** as new potential TRβ-selective thyromimetics.

1. Introduction

Thyroid hormones (THs) are essential regulatory molecules for normal growth and development and for maintaining metabolic homeostasis [1]. Most of the activities elicited by THs are mediated by nuclear thyroid hormones receptors (TRs), which are members of the nuclear hormone receptor family and act as ligand-activated transcription factors. There are two main TR isoforms encoded on separate genes, namely TRα and TRβ. Both TR isoforms bind 3,5,3′-triiodothyronine (T3) and mediate TH-regulated gene expression through interactions with DNA response elements and with a complex array of transcriptional cofactors, including corepressors (CoRs), coactivators (CoAs), integrators like CREB-binding protein (CBP), and general transcription factors (GTFs) [2]. TH/TR binding exerts profound effects in several physiological processes. In the central nervous system (CNS) THs signaling is involved in development and maintenance of brain function, influencing various activities such as neuronal and glial cell differentiation, myelination, and neurogenesis [3,4]. In the liver, THs influence hepatic lipid metabolism through multiple pathways, with insightful effects on energy expenditure [5], fat oxidation [6] and cholesterol

* Corresponding author. Department of Pharmacy, University of Pisa, Pisa, 56126, Italy.
** Corresponding author. Department of Pathology, University of Pisa, Pisa, 56126, Italy.
E-mail addresses: grazia.chiellini@unipi.it (G. Chiellini), simona.rapposelli@unipi.it (S. Rapposelli).
[1] M.R and S.S equally contributed.

https://doi.org/10.1016/j.ejmech.2019.112006
0223-5234/

metabolism [7]. Conversely, alteration of cellular TH signaling in the liver plays a key role in the onset or progression of several liver-associated diseases, such as non-alcoholic fatty liver disease (NAFLD), and hepatocellular carcinoma (HCC) [8]. Therefore, modulating the function of THs offers the potential to treat a wide variety of liver diseases and cancer, as well. Unfortunately, the use of THs as therapeutic agents is hampered by the lack of selectivity and the consequent adverse side effects (such as increased heart rate, cardiac hypertrophy, muscle wasting, and reduced bone density) that are mainly due to their binding to TRα receptors. In order to overcome these drawbacks, selective activation of the β thyroid hormone receptor (TRβ) is an appropriate method to develop new treatments for several chronic diseases with a reduced side effect profile.

During the past two decades, a number of selective TRβ agonists have been developed. These include the analogues Sobetirome (GC-1), KB-141 and the Hep-Direct prodrug VK2809 that exhibits most of the beneficial properties of T3 in the absence of deleterious effects [9–11]. GC-1 emerged in 1995 [9] as the first halogen free thyromimetics. It was shown to bind preferentially to TRβ vs TRα and was initially studied as an hypocholesterolemic compound able to stimulate hepatic pathways without harmful side effects [12]. Due to the beneficial effects of GC-1 and KB2115, the latter known as Eprotirome, entered human clinical trials for dyslipidaemia, and yielded encouraging results in the absence of harmful effects typically associated with THs high levels (for reviews, see Tancevski et al., 2011 [13], Meruvu et al., 2013 [14]). The progression of GC-1 was discontinued despite a promising phase I trial for the treatment of lipid metabolism disorders and obesity, with no phase II trials being planned. Additional applications of GC-1 have been proposed in orphan indications and this drug is now in phase I/II trial for a rare disease (X-Linked Adrenoleukodystrophy) (Clinicaltrial.gov Identifier: NCT03196765). Eprotirome, progressed to phase III clinical trial but was terminated due to unexpected side effects in animal studies [15]. Another selective thyromimetic, namely Resmetirom (MGL-3196) was designed as a liver-specific TRβ agonist able to reduce hepatic lipid synthesis and has progressed to phase II trials (ClinicalTrials.gov Identifier: NCT02912260). In addition, VK2809 is a novel liver-directed thyroid receptor beta agonist pro-drug [16] that possesses selectivity for liver tissue, and after undergoing cleavage by a cytochrome P450 enzyme, is able to release the selective thyromimetic MB07344 which binds to TRβ receptor (Fig. 1). Currently, VK2809 has progressed to Phase 2 clinical trial in patients with primary hypercholesterolemia and non-alcoholic fatty liver disease (NAFLD). (ClinicalTrials.gov identifier: NCT02927184). Although many thyromimetics are currently in clinical trials, none have been approved by FDA (Fig. 1).

Despite the challenges with progressing TRβ selective agonists due to their side effect profiles, their use to treat other human pathologies could be explored as part of drug repositioning strategies. Accordingly, the identification of novel agonists with selectivity for both the TRβ and the liver could represent a valid strategy to regulate metabolic disorders. This paper reports the results of the design and synthesis of a novel series of TRβ agonists. The thyromimetic-analogues were evaluated for their off-target and ADME-Tox properties and the most optimal compounds progressed to in vitro profiling in a nuclear receptor coregulator assay (Thermofisher®) and for their ability to promote lipolysis in human hepatoma cells (HepG2). Further investigation to determine the cellular pathways involved in their lipid-lowering ability was also carried-out. Additionally, to rationalize the pharmacological results, in silico docking studies on selected compounds were also performed in order to simulate their interaction with the putative receptor-binding site. Finally, we performed preliminary in vivo studies to assess the effect of two thyromimetics (compound **3** and its pro-drug **1**), which were shown to be associated with the most optimal off-target and ADME-Tox profile, to determine their ability to modulate cholesterol serum levels, triglicerides, glucose, bilirubin and transaminases in rats.

2. Results & discussion

2.1. Rational design of new thyromimetic molecules

Our search for therapeutic agents focused on the design and synthesis of agonists endowed with high selectivity for TRβ and enhanced hepato-specificity. To this end, we designed and synthesized a new class of thyromimetics based on a diphenylmethane scaffold. This moiety has been widely recognized as an effective replacement for the biaryl-ether core of THs [16–20]. Notably, in previously developed diphenylmethane-based thyromimetics, the oxyacetic acid side chain was shown to have a critical role in conferring TRβ selectivity [19]. On the basis of this finding, we designed compounds **1**–**4** and **9**–**11** (Fig. 2). In compounds **3**, **4**, **9** and **10**, the hydroxyl group at the 4′-position in T3 was replaced by an amino group. This type of modification generates the zwitterion that could be detrimental for the bioavailability of the molecule. Hence, we synthesized the corresponding acetamide-analogues of **3** and **4**, namely **1** and **2**, which could represent potential pro-drugs with improved drug-like properties. Oral administration of these pro-drugs, by first pass metabolism through the liver, should lead to an efficient generation of the corresponding parent compounds. Based on our previous experience gained during the development of SG-compounds as thyronamine analogues of T1AM, it is known that the oxyethylamine sidechain represents a valid precursor of the oxyacetic group that is formed following the metabolic activation by MAOs [18]. Therefore, we synthesized the derivatives **5**–**8** as possible precursors of the corresponding thyromimetics with an oxyacetic structure. The two iodine atoms present in the T3 inner ring have been replaced with hydrogen atoms (**2** and **4**), with two methyl groups (**1**, **3**, **5**, **7**, **10** and **11**) or with a hydrogen and CF_3 (or H and F) as in compounds **6**, **8** and **9**. As to the iodine atom in the outer ring of T3, it has been replaced by an isopropyl group (**1**–**6**) or by a hydrogen atom (**7**–**11**).

2.2. Chemistry

A crucial component in our synthetic procedures is the synthesis of the biphenylmethane scaffold which was obtained with the palladium (0)-catalyzed Suzuki-Miyaura cross coupling reaction between the substituted benzylbromide and selected phenyl boronic acid derivatives. The Suzuki-Miyaura reaction was performed under standard or microwave-assisted conditions, with yields ranging from 22% to 60% as reported in Table 1. In particular, benzylbromide **15**, which was not commercially available, was obtained as shown in Scheme 1. A one-pot reaction between 2-isopropylaniline, acetic anhydride, and bromine was carried out in acetic acid providing the bromobenzene derivative **12** with high yields. Then, formylation of **12** with n-BuLi and DMF at −78 °C led to benzaldehyde-derivative **13**, which was reduced with $NaBH_4$ to provide the benzylic alcohol **14**. Finally, **15** was obtained by bromination of **14**, using CBr_4 and PPh_3 (Appel reaction).

Scheme 2 illustrates the synthetic procedure to obtain compounds **1**–**6**. Briefly, phenol derivatives **19**–**21** were obtained by demethylation of purified cross coupling products **16**–**18** by using BBr_3. The following O-alkylation reaction of **20** and **21** with bromoacetic acid led to compound **1** and **2**, which have undergone deacetylation in presence of hydrochloric acid at concentrated grade to provide desired compound **3** or **4**. Compounds **5** and **6**

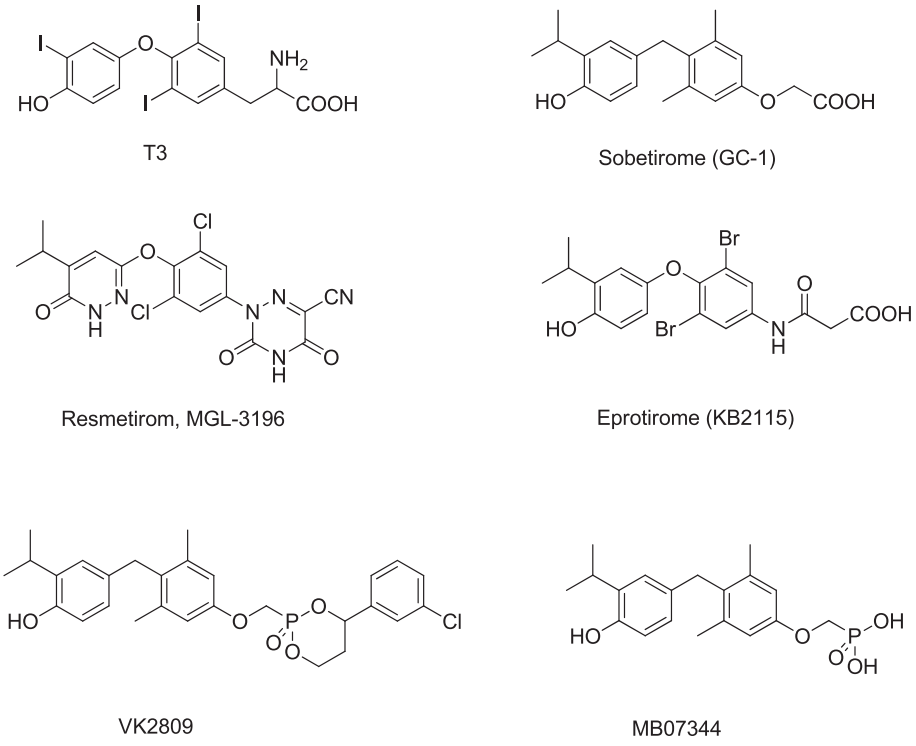

Fig. 1. Structures of TRβ agonists which have been progressed in drug discovery.

were obtained by reaction of phenolic derivative **19** or **21** with bromoacetonitrile, followed by reduction of intermediates **22** and **23** in presence of $LiAlH_4$ and $AlCl_3$.

Compounds **7**–**11** were obtained according to the synthetic procedure reported in Scheme 3. Briefly, purified cross-coupling products **24**–**26** were treated with BBr_3 to afford the phenol derivatives **27**–**29** which have undergone O-alkylation reaction with bromoacetonitrile or ethyl bromoacetate leading to intermediates **30**–**32** and **33**, respectively. Compound **9** was obtained by selective nitro-group reduction (**35**), followed by acid hydrolysis with HCl at concentrated grade. Treatment of **33** with hydrazine and $FeCl_3$ led to ethyl ester **36** which was converted to compound **10** by mild saponification. Finally, the conversion of amine moiety of **10** to a phenolic group using diazonium salt led to compound **11**.

2.3. Off-target and ADME-Tox profiling

In order to identify the most promising compound for

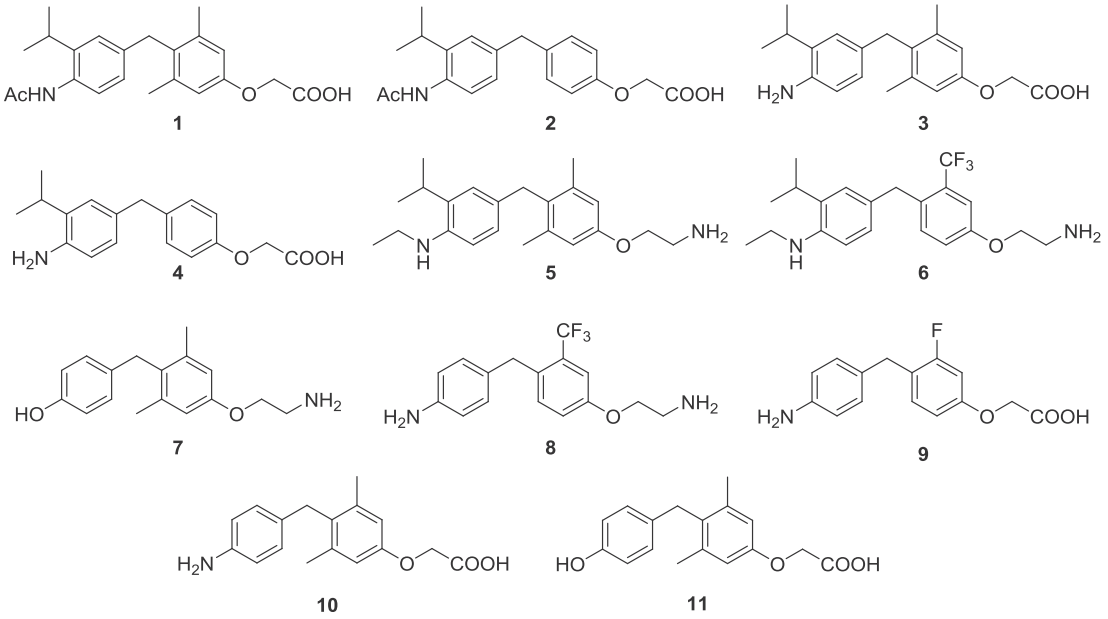

Fig. 2. Structures of novel thyromimetics **1**–**11** with a biphenylmethane scaffold.

Table 1
Cross-Coupling Reactions. [a]commercially available starting material; [b]compound **15**; [c]reaction was performed using a microwave reactor; [d]yields refer to products after compound purification which was performed by flash chromatography (for further information on eluent mixture, consult supplementary material).

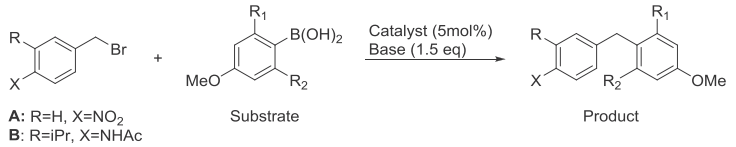

A: R=H, X=NO_2
B: R=iPr, X=NHAc

Substrate | Substrate[a] | | | | | | | | |

Entry	R1	R2	Product	Base	Catalyst	Solvent	Temp.	Time	Yield[d]
B[b]	Me	Me	**16**	K_2CO_3	$PdCl_2$	acetone/H_2O	40 °C	6h	60%
B[b]	H	H	**17**	K_2CO_3	$PdCl_2$	Acetone/H_2O	100 °C	10'[c]	30%
B[b]	CF_3	H	**18**	K_2CO_3	$Pd(PPh_3)_4$	1,4 dioxane	90 °C	12h	22%
A[a]	F	H	**24**	$Ba(OH)_2$*$8H_2O$	$Pd(PPh_3)_4$	1,2-DME/H_2O	110 °C	20'[c]	39%
A[a]	CF_3	H	**25**	K_2CO_3	$Pd(PPh_3)_4$	1,4 dioxane	90 °C	6h	52%
A[a]	Me	Me	**26**	K_2CO_3	$PdCl_2$	acetone/H_2O	rt	72h	32%

progression in the drug discovery process, the novel thyromimetics **1**–**11** were screened in vitro at 10 μM against a panel of early ADME-Tox assays comprising cytotoxicity (U2OS, HEK, hTERT and MCF-7), cardiotoxicity (*h*ERG), cytochrome P450 inhibition (CYP1A2, CYP2C9, CYP2C19, CYP2D6 and CYP3A4), and off-targets such as Aurora B kinase and phosphodiesterase (PDE4C1), and epigenetic enzymes (SIRT7, HDAC4, HDAC6, HDAC8 and HDAC9), see Fig. 3. At first, the cytotoxicity of **1**–**11** were determined after 24 h or 48 h of treatment in the four cell-lines. Reassuringly, only compound **6** was associated with a low degree of cytotoxicity at

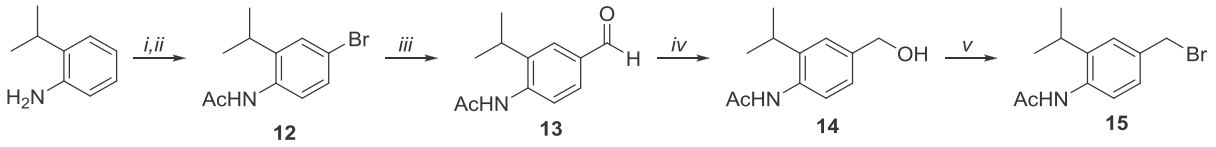

Scheme 1. Synthesis of benzylbromide **15.** *Reagents and conditions. i:* Ac_2O, AcOH, 117–118 °C, 1 h; *ii*: Br_2, AcOH, 65 °C, 30'; *iii:* n-BuLi, DMF, THF, −78 °C → rt, 3 h; *iv:* $NaBH_4$, MeOH, 0 °C → rt, 12 h; *v:* CBr_4, PPh_3, DCM, 0 °C → rt, 12 h.

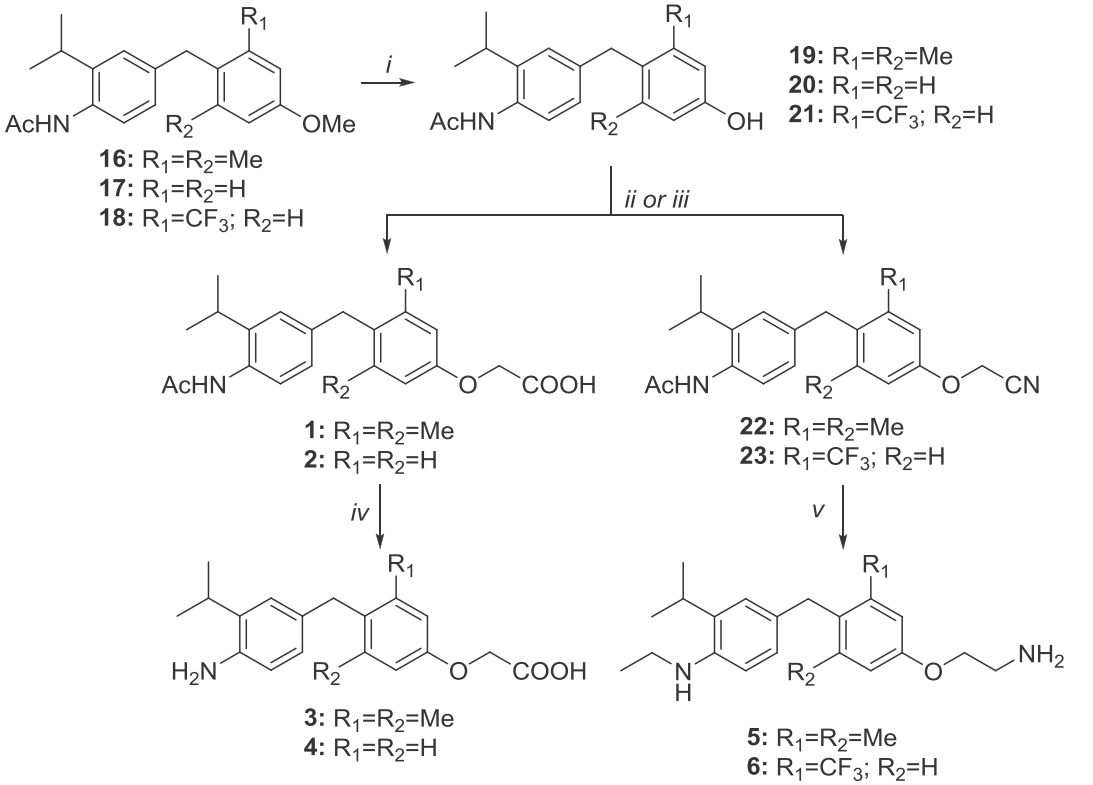

Scheme 2. Synthesis of final compounds **1**–**6**. *Reagents and conditions.* (*i*) BBr_3, DCM, −10 °C, 1 h; (*ii*) $BrCH_2COOH$, DMF, Cs_2CO_3, rt, 1 h; (*iii*) $BrCH_2CN$, DMF, Cs_2CO_3, rt, 30'; (*iv*) HCl 37%, H_2O, 120 °C, 12 h; (*v*) $LiAlH_4$, $AlCl_3$, THF, rt → 66 °C, 12 h.

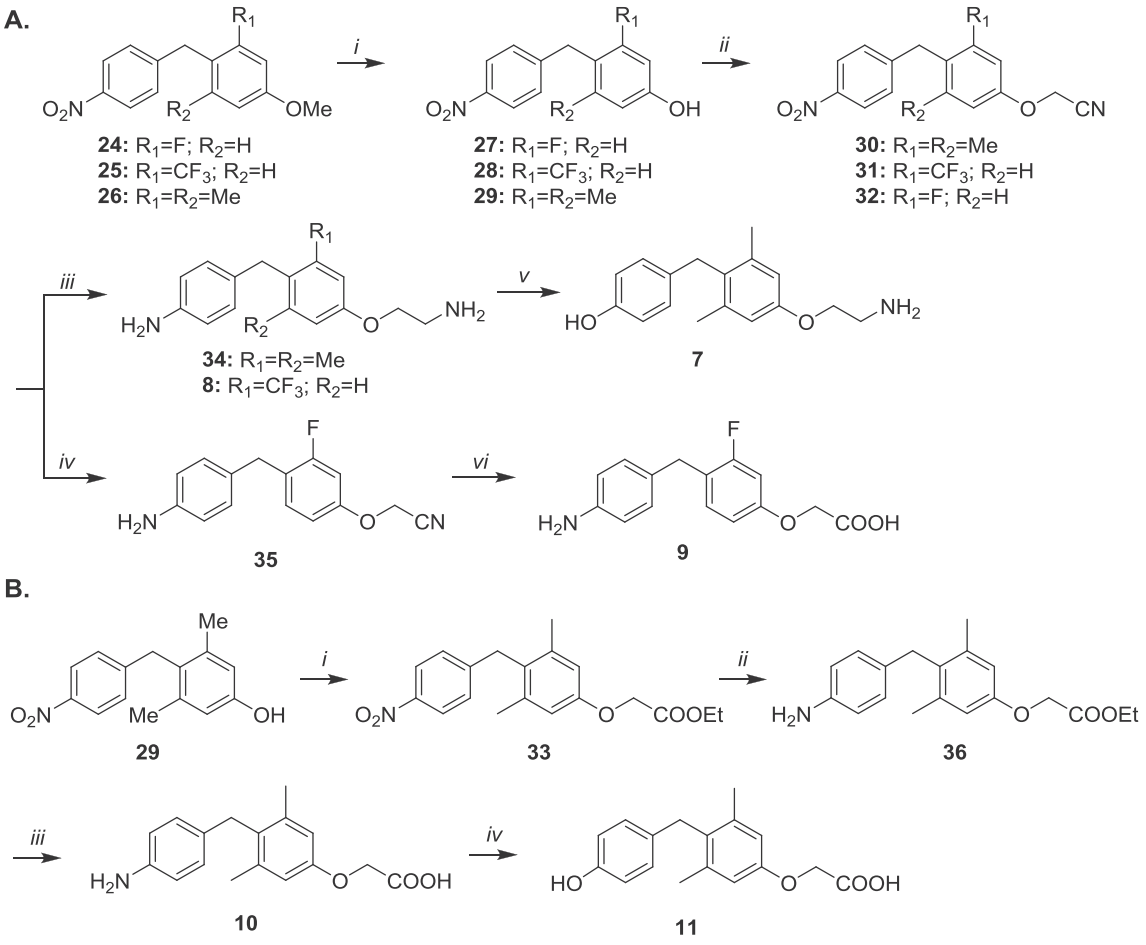

Scheme 3. Synthesis of final compounds **7**–**11**. *Reagents and conditions*: **A.** (*i*) BBr_3, DCM, −10 °C, 1 h; (*ii*) $BrCH_2CN$, DMF, Cs_2CO_3, rt, 20′, 1 h; (*iii*) $LiAlH_4$, $AlCl_3$, THF, rt → 66 °C, 12 h; (*iv*) H_2, Pd/C, MeOH, 12 h; (*v*) H_2SO_4, $NaNO_2$, H_2O, 100 °C, 1 h; (*vi*) HCl 37%, H_2O, 100 °C, 4 h; **B.** (*i*) $BrCH_2COOEt$, DMF, Cs_2CO_3, rt, 1 h; (*ii*) H_2, Pd/C, EtOH, 150′, rt (*iii*) NaOH 10%, MeOH, 66 °C, 1 h; (*iv*) H_2SO_4, $NaNO_2$, H_2O, 100 °C, 1 h.

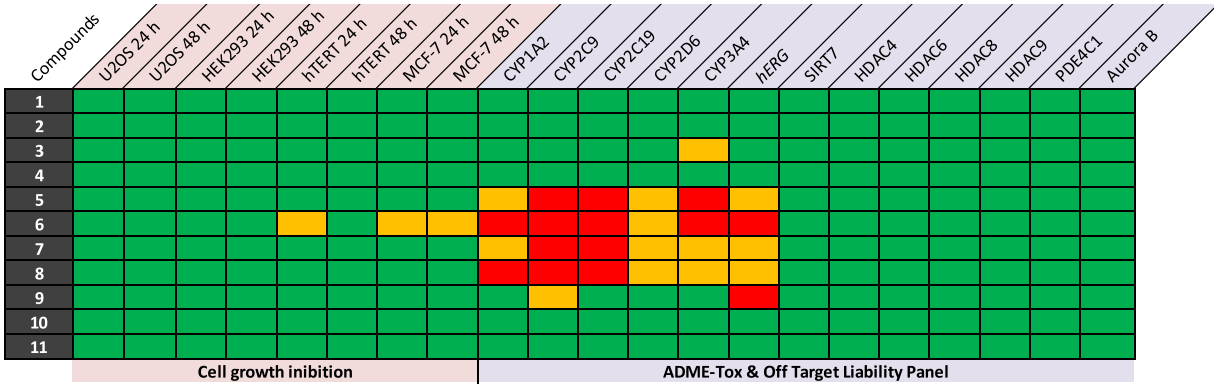

% Inhibition at 10 μM [compound]	Classification
<50	Acceptable profile
51-90	A flag that requires remedial action
>91	Major issue that requires significant attention

Fig. 3. Off-target and ADME-Tox profile of compounds **1**–**11**. All compounds were screened at 10 μM in triplicate. A traffic-light system was used to characterize the effect of the new thyromimetics in the in vitro off-target and ADME-Tox assays.

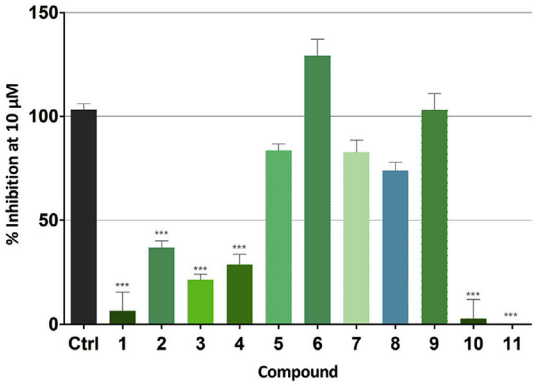

Fig. 4. hERG ion-channel inhibition profile of compounds **1**–**11**. All compounds were tested at 10 μM in triplicate, and raw data were normalized to positive control (Ctrl = Compound E–4051) and negative control (DMSO) and the % Inhibition of the hERG ion-channel activity calculated. Results were compared to control using the One-Way ANOVA test. ***$p < 0.005$.

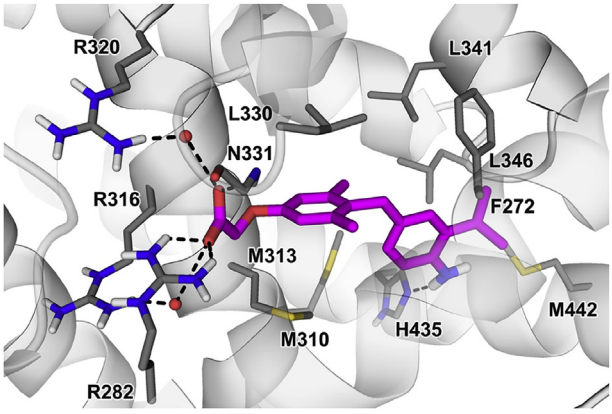

Fig. 5. Binding mode of compound 3 in the TRβ LBC. The receptor is displayed in grey cartoon, while the ligand and the main protein residues are depicted in magenta and grey sticks respectively. H3 helix and the N331 loop are in transparency and non-polar hydrogens are omitted for sake of clarity. H-bonds are shown as black dashed lines.

10 μM (65% at 24 h and 53% at 48 h) towards MCF-7 cell-line (see "paper data in brief" for details). [Ref].

The ADME-Tox profile of a compound is a major factor when selecting the best candidate(s) to progress in the drug discovery value chain. Among several enzymes responsible for xenobiotic transformation, the cytochrome P450 (CYP450) enzyme plays a key role in phase I oxidative metabolism and most of drug biotransformation are essentially achieved by five isoforms: CYP1A2, CYP2C9, CYP2C19, CYP2D6, and CYP3A4 [21]. Interestingly, while the carboxylic compounds were associated with minimal adverse effect on CYP450 enzyme activity, compounds **5**–**8** yielded considerably more inhibition against all CYP450 enzymes, probably as a consequence of the oxyethylamine moiety. In order to assess the off-target liability of newly synthesized molecules, all compounds were tested against several well-known off-targets. For this study, enzymes belonging to different classes were selected. SIRT7, HDAC4, HDAC6, HDAC8 and HDAC9 were chosen as representatives of an undesirable epigenetic modulation [22,23]. No compounds were associated with adverse inhibition of these targets. Moreover, the new synthesized molecules were also shown to be inactive against Aurora B kinase and PDE4C1 enzymes which are known to be essential for cell growth and whose inhibition has been involved in tumorigenesis. Finally, the ability of the newly synthesized molecules to modulate hERG ion-channel activity was assessed using the Predictor hERG FP assay (Thermofisher®). The hERG ion-channel plays a key role in cardiac action potential and represents one of the main reasons for failure of clinical candidates or, even worse, a cause for withdrawal of drugs from the market. For this reason, it is considered important to assess the effect of compounds on hERG ion-channel activity at an early stage of drug discovery process. Compounds **1**–**4**, **10** and **11** did not significantly alter the hERG ion-channel activity, such that the percentage of inhibition was <40% at 10 μM. More importantly, compound **1**, **10**, and **11** were shown to inhibit hERG ion-channel activity <25% at 10 μM (Fig. 4). Overall, the off-target and ADME-Tox profiling led to the identification of 6 compounds (**1**–**4**, **10**, **11**) with the most optimal profiles for progression. Next, we proceeded with biological evaluation to assess their agonist activity against TRα and TRβ.

2.4. Nuclear receptor activation

The activity of compounds **1**–**4** and **10**–**11** on TRα and TRβ was assessed using the LanthaScreenTM TR-FRET Nuclear Receptor Coregulator Assay (service provided by Invitrogen Corporation, USA) in 10-point dose-response experiments for each compound. Among the tested compounds, only **3** and **11** were active against TRα and TRβ. Interestingly, compound **11** activated both TR isoforms with EC50 towards TRα and TRβ of respectively 54 and 32 nM. Apart from ability to activate the receptors, the selectivity towards the TRβ isoform is pivotal in order to avoid side effects related to TRα activation in vivo. Above all, compound **3** was shown to be a TRβ agonist with EC50 value 458 nM, whereas it only activated TRα to 30% (at 1 μM) (see Supporting Information for details). Based upon these results, compound **3** was selected for further biological investigations. In addition, compound **1** was also selected for further study, as it was originally designed as pro-drug of compound **3**, and more importantly, it was also found to possess an acceptable off-target and ADME-Tox profile.

2.5. Computational studies

In order to elucidate the activity and the preferential binding of compound **3** for TRβ with respect to TRα, docking calculations were carried out with the aid of Glide 6.7 (Maestro packaging) into the ligand-binding-cavity (LBC) of the two receptors, using the structures co-crystallized with GC-1, PDB: 3ILZ and 3IMY, respectively (See Experimental Section for X-ray selection). Bearing in mind the importance of water-mediated interactions for GC-1, which is a potent thyromimetic as well as a very close analogue of **3**, our calculations were performed retaining crystal water molecules within 3 Å of the ligand. As for TRβ, the best ranked docking pose predicted for **3** (Fig. 5) is highly superimposable with the crystal structure of GC-1 into the thyroid receptor. Specifically, the ligand carboxylate forms a H-bond with the backbone NH group of the N331 and engages two charge-reinforced H-bonds with the guanidinium group of R282. Moreover, water-mediated contacts are found with the R316 and R320 side chains. As for the dimethyl phenyl moiety, it establishes many van der Waals interactions with the LBC lipophilic side chains of L330, I275, I353, M313 and M310 and, thanks to the 3,5 di-methyl substitutions, it is locked in the active perpendicular conformation with respect to the terminal phenyl ring [24]. Other profitable lipophilic interactions are detected between the latter and the L341, F272, I276, L346 side chains and between the iso-propyl substituent with the residues F269, F272, M442, L346 and F451. Finally, the **3** amino group H-bonds the imidazoline nitrogen atom of the H435. Of note, when the zwitterionic form of **3** is docked into the receptor, numerous bad contacts are found between the cationic amino group and the

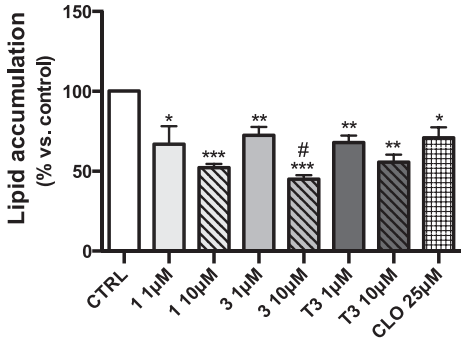

Fig. 6. Effects of **1** and **3** on total lipid accumulation in HepG2 cells. Cells were treated for 24 h with **1**, **3** or **T3** at 1 and 10 μM 25 μM Cloroquine (CLO) was used as positive control. Oil red O stained intercellular oil droplets were eluted with isopropanol and quantified by spectrophotometry analysis at 510 nm. Values represent the mean ± SEM of 4–8 experiments. The groups were compared using the One-Way ANOVA followed by Tukey's range test. *p < 0.05 *vs.* Ctrl; **p < 0.01 *vs.* Ctrl; ***p < 0.005 *vs.* Ctrl; #p < 0.05 *vs.* **3** 1 μM.

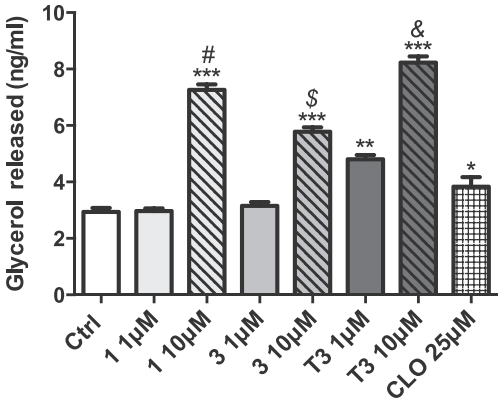

Fig. 7. Thyromimetic-derivatives **1** and **3** induce lipolysis in HepG2 cells. Glycerol released in the culture medium (0.5 mL) of HepG2 cells after 24 h treatment with **1**, **3** and **T3** at 1 and 10 μM 25 μM Cloroquine (CLO) was used as positive control. Values represent the mean ± SEM of 4–8 experiments. The groups were compared using the One-Way ANOVA followed by Tukey's range test. *p < 0.05 *vs.* Ctrl; **p < 0.01 *vs.* Ctrl; ***p < 0.005 *vs.* Ctrl; #p < 0.005 *vs.* compound **1** 1 μM; $p < 0.01 *vs.* compound **3** 1 μM; &p < 0.01 *vs.* **T3** 1 μM.

surrounding lipophilic residues of the LBC, which might be responsible of the lower activity of **3** with respect to its hydroxyl analogue GC-1 (data from the literature). Moreover, the bulkiness of the residues F269, F455 and F439 does not allow a proper accommodation of the 4′–NH–acetyl group of compound **1**, generating intramolecular steric clashes and hampering the formation of an H-bond with H435, justifying the loss of activity of this prodrug (see Figure SI2 together with comments on the other derivatives of the series that can be found in Supporting Information).

As for the selectivity profile of **3**, in TRα a pose very similar to the co-crystallized structure of GC-1 with the receptor is found. This outcome is not surprising since it is known that only a single residue mutation (S277 in TRα versus N331 in TRβ) differentiates within the TRα and TRβ binding pockets, and this mutation does not alter the overall shape and characteristics of the two clefts. However, a deeper analysis shows that our ligand is not able to interact with R262 (R316 in TRβ) and just one water-mediated contact is found with the R228 side chain (R282 in TRβ). In this regards, crystallographic analysis and MD studies [25,26], have demonstrated that this single mutation is able to affect the orientation of one of the interacting arginines (R228 in TRα and R282 in TRβ). Specifically, in TRβ, the N331 side chain interacts with the R282 guanidinium, which in turn is permanently and optimally oriented toward the ligand carboxylate allowing GC-1 to stabilize a rich H-bonds network with the three surrounding arginines, justifying its preferential binding to TRβ. As described above, analogously to GC-1, thyromimetic compound **3** is able to establish a broad and stable interaction pattern with TRβ arginines, including strong and direct contacts with R282, while part of these interactions are lost in TRα. Reasonably, this might in part justify the preferential binding of **3** to TRβ with respect to TRα. Also, it is known that in TRβ LBC, the residues lining the outer ring of thyromimetics (especially the M442 residue) [27], are more flexible with respect to their corresponding TRα residues, so that large 3′-substituents and certain 4′-substituents [28], increment selectivity toward this isoform. Thus, it is possible that **3**, possessing the novel combination of 3′-iPr e 4′-NH_2 substituents on the outer ring, it is better accommodated within the TRβ pocket.

2.6. Effects on lipid metabolism

Abnormal accumulation of lipids in hepatocytes is a prominent aspect in several liver diseases such as NAFLD (non-alcoholic fatty liver spectrum disease) and alcoholic steato-hepatitis (ASH) [29]. In order to investigate whether the new thyromimetic molecules **1** and **3** could promote lipolysis, and whether derivative **1** is capable of efficiently delivering the corresponding parent compound **3**, we evaluated their effect on lipid metabolism in the human hepatoma cells HepG2. Initially HepG2 cells were incubated for 24 h with **1** and **3** at 1 μM and 10 μM, with T3 as reference drug (Fig. 6). Oil-red O staining was used to monitor intracellular lipid accumulation (Fig. 7). Cloroquine (CLO) 25 μM was used as positive controls.

Oil Red O staining revealed that the newly designed compound **3** reduced total lipid accumulation into lipid droplets with a potency comparable or even higher than equimolar doses of T3 (Fig. 6). This result also shows that compound **1** exerts the same effect of **3** in reducing lipid accumulation, whereas the increase in glycerol released levels seems to be more efficient when compared with **3**. This result let us to speculate that thyromimetic derivative **1** is a pro-drug which possesses improved drug-like properties when compared to **3** (zwitterionic molecule) and this contributes to increase the bioavailability of the molecule inside the hepatocytes. Further pharmacokinetic investigations need to be carried out in the near future to confirm our hypothesis.

2.7. Effects on AMPK/ACC pathway

Thyroid hormone mediates lipogenesis, fatty acid β-oxidation, cholesterol synthesis and the reverse cholesterol transport pathway through different mechanisms such as (a) the induction of genes transcription involved in metabolism as well as (b) the activation of alternative cellular pathways implicated in the direct catabolism of fatty acids, such as autophagy [30,31]. Hepatic autophagy regulates lipid metabolism through elimination of triglyceride accumulation in liver and prevents the development of steatosis [30,32]. The 5′ AMP-activated protein kinase (AMPK) is a serine/threonine protein kinase which plays a central role in regulating cellular metabolism and energy balance in mammalian cells [33]. Once activated, AMPK triggers several pathways such as glycolysis, fatty acid oxidation, and lipolysis. The overall effect on lipid metabolism is stimulation of fatty acid oxidation (FAO) and inhibition of cholesterol and triglycerides synthesis [34]. Since AMPK is a regulator of autophagy [35,36], we investigated AMPK as a possible target of thyromimetic analogues **1** and **3**. In particular, we examined the protein levels of phosphorylated AMPK (p-AMPK), and its target phosphorylated acetyl-CoA carboxylase (p-

ACC), a rate-limiting enzyme in cholesterol and fatty acid biosynthesis. As shown in Fig. 8, both compounds, when tested at the higher concentration (i.e. 10 μM), induced a significant enhancement of p-AMPK/AMPK and p-ACC/ACC ratios. Consistently, the effect induced by thyromimetic analogue **1** in the p-ACC/ACC ratio was more pronounced than that observed with the thyroid hormone T3.

2.8. Lack of hepatic toxicity and cardiac hypertrophy in thyromimetics-treated rats

Our in vitro results showed that compound **3** and its pro-drug **1** efficiently reduced lipid accumulation, suggesting their potential therapeutic use in pathological conditions, such as NAFLD. To assess their effect in vivo we treated F344 male rats for 3 days with daily intragastric (IG) administrations of **1** or **3** (50, 75 and 100 μg/100 g b. w.). Two additional groups treated with the vehicle or with T3 (20 μg/100 g b. w.) were included. As shown in Fig. 9A, despite the brief exposure, T3 caused a significant increase of heart weight, as well as of the heart/body weight ratio. No such effect was found in the heart of animals treated with **1** or **3** at all doses used (Fig. 9A), showing that the preferential binding to - and activation of - TRβ does not result in cardiac hypertrophy. As to the liver, while T3 treatment caused a significant reduction of the liver weight/body weight ratio, neither **1** nor **3** caused change in liver weight. Similar results were obtained when the two thyromimetics were administered at the dose of 75 μg/100 g b. w. intraperitoneally for 3 days (Fig. 9B). Notably, no change in the serum levels of markers of liver injury, such as transaminases or bilirubin was observed following administration of the two thyromimetics. Interestingly, the two novel drugs did not exhibit any significant effect on serum levels of cholesterol and glucose, whereas compound **1** induces a significant reduction of triglycerides when compared to controls and to T3 (Table 2).

3. Conclusion

Compound **3** and its pro-drug **1** showed encouraging off-target and ADME-Tox profile that prompted us to explore them as TRβ selective thyromimetics. The biochemical-based nuclear receptor assay allowed us to consider compound **3** as a potential TRβ selective agonist able to influence lipid metabolism and fat oxidation in hepatocytes. Indeed, our in vitro assays showed that both compound **3** and its pro-drug (**1**) were able to reduce lipid accumulation in HepG2 and promote lipolysis with comparable effects to those elicited by T3, used as reference drug. These results were associated with a safe off-target and ADME-Tox profile. Importantly, in vivo studies confirmed the apparent lack of toxicity of our thyromimetics. Indeed, no liver injury, as assayed by serum levels of ALT, AST and bilirubin and no cardiac hypertrophy, a critical side effect of T3, could be observed in thyromimetic-treated rats. Interestingly, we found a significant decrease in blood triglyceride content following administration of both TRβ agonists, suggesting their possible effect on lipid metabolism. Future in vivo studies will be needed to investigate the effect of both compounds in experimental models of NAFLD in order to validate them as new tools to treat hepatic diseases and to confirm that **1** is an efficient pro-drug of TRβ selective agonist **3**, with higher affinity toward the liver.

4. Experimental section

4.1. Chemistry

4.1.1. General material and methods

Melting points were determined on a Kofler hot-stage apparatus and are uncorrected. Chemical shifts (δ) are reported in parts per million downfield from tetramethylsilane and referenced from solvent references; coupling constants *J* are reported in hertz. ^{1}H NMR, ^{13}C NMR and ^{19}F NMR spectra were obtained with a Bruker TopSpin 3.2400 MHz spectrometer and were recorded at 400, 101 and 376 MHz, respectively. ^{19}F and ^{13}C NMR spectra are ^{1}H decoupled. ^{19}F NMR spectra are unreferenced, corrected from

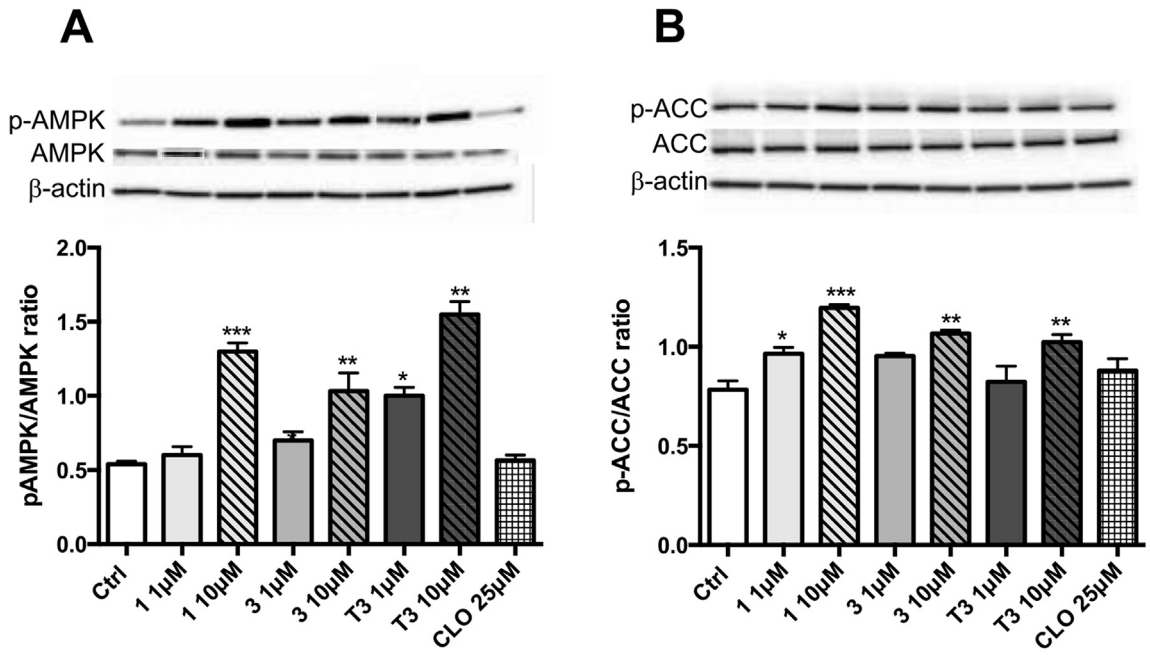

Fig. 8. Derivatives **1** and **3** regulate metabolism in HepG2 cells via AMPK/ACC pathway. (A) Representative immunoblotting images and quantitative analysis of AMPK phosphorylation. (B) Representative immunoblotting images and quantitative analysis of ACC phosphorylation. *p < 0.05 *vs.* Ctrl; **p < 0.01 *vs.* Ctrl; ***p < 0.005 *vs.* Ctrl.

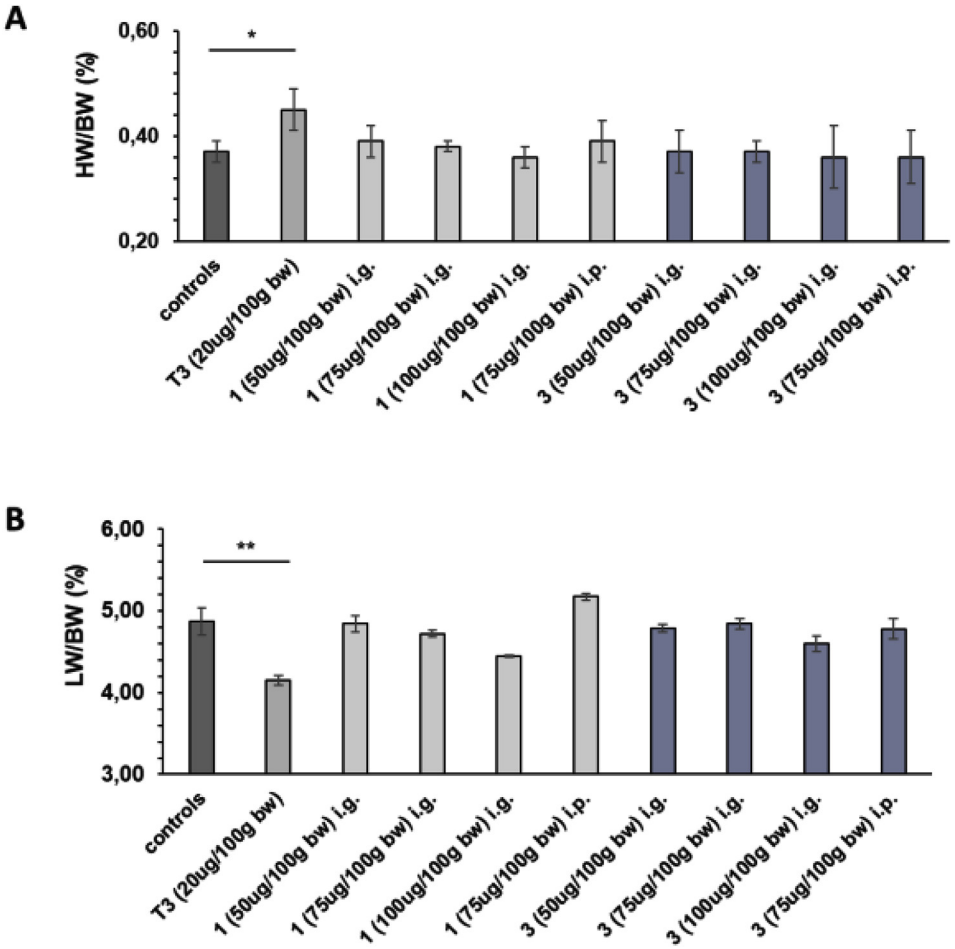

Fig. 9. Effect of T3, **1** and **3** on liver/body weight ratio. F344 male rats were treated for 3 days with daily intragastric (IG) injections of **1** or **3** (50, 75 and 100 μg/100 g b. w.) or T3 (20 μg/100 g b. w.). A control group received the vehicle (DMSO 5% in corn oil). Additional two groups received daily injections of either **1** or **3** at the dose of 75 μg/100 g b. w. intraperitoneally for 3 days. **P < 0.01.

Trifluoroacetic Acid (TFA) as external standard (−76.2 ppm). Signal spectra were fully decoupled. The following abbreviations are used: singlet (s), doublet (d), triplet (t), double−doublet (dd), and multiplet (m). The elemental compositions of the compounds agreed to within ±0.4% of the calculated values. Chromatographic separation was performed on silica gel columns by flash (Kieselgel 40, 0.040−0.063 mm; Merck) or gravity column (Kieselgel 60, 0.063−0.200 mm; Merck) chromatography. The ≥95% purity of the tested compounds was confirmed by combustion analysis. Reactions were followed by thin-layer chromatography (TLC) on Merck aluminum silica gel (60 F254) sheets that were visualized under a UV lamp. The microwave-assisted procedures were carried out with a Biotage Initiator + microwave. Evaporation was performed in vacuo (rotating evaporator). Sodium sulfate was always used as the drying agent. Commercially available chemicals were purchased from Sigma-Aldrich or Fluorochem.

4.1.1.1. Synthesis of 2-(4-(4-acetamido-3-isopropylbenzyl)-3,5-dimethylphenoxy)acetic acid (1). A solution of phenolic derivative **19** (0.29 mmol) in DMF was treated with Cs_2CO_3 (473 mg;

Table 2
Effect of thyromimetics **1** and **3** and **T3** on rat Serum Levels of AST/GOT, ALT/GPT, Bilirubin, Cholesterol and Triglycerides (TGs) after the treatment with **1** or **3** (i.g., 50, 75 and 100 μg/100 g b.w; or i.p. 75 μg/100 g b.w.) or T3 (20 μg/100 g b.w.) for 3 days.

Treatment	AST/GOT (U/L)	ALT/GPT (U/L)	Bilirubin (mg/dl)	Glucose (mg/dl)	Cholesterol (mg/dl)	TGs (mg/dl)
Controls	153 ± 11	46 ± 4	1.4 ± 0.2	151 ± 13.5	67.2 ± 2.5	86.8 ± 10.4
T3	159 ± 11	53 ± 4.1	1.4 ± 0.3	139 ± 4.4	65.2 ± 7.1	90.2 ± 9.3
1 i.g. (50 μg/100 g)	141 ± 11	46 ± 3.1	1.1 ± 0.3	129 ± 14	68.0 ± 5.2	70.4 ± 7.6
1 i.g. (75 μg/100 g)	133 ± 8	46 ± 1.7	0.9 ± 0.1	132 ± 7.6	71.4 ± 6.6	67.0 ± 12.0
1 i.g. (100 μg/100 g)	108 ± 7	37 ± 2.5	1.1 ± 0.2	164 ± 12	67.6 ± 8.1	62.8 ± 6.1*
3 i.g. (50 μg/100 g)	134 ± 6	41 ± 2.1	1.3 ± 0.3	136 ± 6	69.5 ± 9.4	68.3 ± 9.1
3 i.g. (75 μg/100 g)	119 ± 6	43 ± 3.3	1.6 ± 0.2	153 ± 18	68.6 ± 5.6	74.0 ± 12.8
3 i.g. (100 μg/100 g)	102 ± 5	42 ± 4.6	1.0 ± 0.2	166 ± 5.1	70.2 ± 7.0	67.8 ± 12.5
1 i.p. (75 μg/100 g)	134 ± 10	38 ± 2.9	1.5 ± 0.4	132 ± 14	71.4 ± 3.1	74.2 ± 9.0
3 i.p. (75 μg/100 g)	123 ± 10	36 ± 1.7	1.1 ± 0.2	129 ± 9	69.6 ± 1.2	79.6 ± 9.7

Values are expressed as means ± S.D. of 3−4 animals per group. *Significantly different from Controls for at least; p < 0.05.

1.45 mmol) and $BrCH_2COOH$ (0.29 mmol). The mixture obtained was stirred for 1 h at rt and then, quenched with water. After extraction with DCM, aqueous phase was acidified with HCl 10% and extracted again with DCM. Organic phases were then collected, dried, filtered and concentrated to obtain a crude which was washed in hexane, providing final compound **1**. Yield: 82% (white powder). ^{1}H NMR (CD_3OD-d_4): δ 1.12 (d, 6H, J = 6.8 Hz, CH_3); 2.12 (s, 3H, CH_3CO); 2.18 (s, 6H, CH_3); 3.05–3.08 (m, 1H, CH); 3.98 (s, 2H, CH_2); 4.35 (s, 2H, CH_2); 6.67 (s, 2H, Ar); 6.76 (dd, 1H, J = 2.0, 8.0 Hz, Ar); 7.00–7.08 (m, 2H, Ar) ppm. ^{13}C NMR (CD_3OD-d_4): δ 180.44 (COOH); 172.91 (CH_3CO); [158.17, 145.59, 140.71, 139.23, 132.96, 130.42, 128.55, 126.41, 126.32, 115.34] Ar; 68.49 (OCH_2); 34.84 (CH_2); 29.06 (CH); 24.18 ($CHCH_3$); 23.70 (CH_3); 22.81 (CH_3CO); 20.52 (CH_3) ppm. Anal. Calcd for $C_{22}H_{27}NO_4$: C, 71.52%; H, 7.37%; N, 3.79%. Found: C, 71.41%; H, 7.42%; N, 3.59%.

4.1.1.2. Synthesis of 2-(4-(4-acetamido-3-isopropylbenzyl)phenoxy) acetic acid (2). The crude product was obtained following the same synthetic procedure reported for compound **1**. The crude was purified by suspension in hexane. Yield: 64% (grey powder). ^{1}H NMR (CD_3OD): δ 1.64 (d, 6H, J = 6.8 Hz, CH_3); 2.13 (s, 3H, CH_3CO); 3.08 (m, 1H, J = 6.8 Hz, CH); 3.89 (s, 2H, CH_2); 4.61 (s, 2H, CH_2COOH); 6.83 (d, 2H, J = 8.4 Hz, Ar); 6.98 (dd, 1H, J = 2.0, 8.0 Hz, Ar); 7.08 (d, 1H, J = 8 Hz, Ar); 7.12 (d, 2H, J = 8.4 Hz, Ar); 7.17 (d, 1H, J = 2 Hz, Ar) ppm. ^{13}C NMR (CD_3OD): δ 172.81 (COOH); 172.71 ($COCH_3$); [157.74, 145.62, 142.06, 135.55, 133.10, 130.74, 128.54, 127.48, 127.16, 115.51] Ar; 65.88 (CH_2COOH); 41.56 (CH_2); 29.02 (CH); 23.59 (CH_3); 22.67 (CH_3CO) ppm. Anal. Calcd for $C_{20}H_{23}NO_4$: C, 70.36%; H, 6.79%; N, 4.10%. Found: C, 70.43%; H, 6.69%; N, 4.21%.

4.1.1.3. Synthesis of 2-(4-(4-amino-3-isopropylbenzyl)-3,5-dimethylphenoxy)acetic acid (3). Compound **1** (103 mg, 0.279 mmol) and HCl conc. (8 mL) were mixed with 2 mL of water and refluxed at 120 °C for 4 h. Upon cooling a solid was formed, mainly constituted by compound **3**. Crude obtained was washed in HCl 10% and hexane under vigorous stirring. Yield: 52% (grey powder). ^{1}H NMR (CD_3OD-d_4): δ 1.15 (d, J = 6.8 Hz, 6H, CH_3); 2.19 (s, 6H, CH_3); 2.92–2.99 (m, 1H, CH); 3.87 (s, 2H, CH_2); 4.67 (s, 2H, OCH_2); 6.52 (dd, 1H, J = 1.8, 8.0 Hz, Ar); 6.61 (d, 1H, J = 8.0 Hz, Ar); 6.62 (s, 2H, Ar); 6.79 (d, 1H, J = 1.8 Hz, Ar) ppm. ^{13}C NMR (CD_3OD-d_4): δ171.77, 157.28, 142.51, 139.50, 134.79, 132.24, 131.59, 126.44, 125.77, 117.72, 115.03, 66.02, 52.53, 34.52, 28.32, 23.05, 20.52 ppm. Anal. Calcd for $C_{20}H_{25}NO_3$: C, 73.37%; H, 7.70%; N, 4.28%. Found: C, 73.52%; H, 7.68%; N, 4.19%.

4.1.1.4. Synthesis of 2-(4-(4-amino-3-isopropylbenzyl)phenoxy)acetic acid (4). The crude product was obtained following the same synthetic procedure reported for compound **3** and purified by resuspension in hexane. Yield: 96% (grey powder). ^{1}H NMR (CD_3OD-d_4): δ 1.26 (d, 6H, J = 6.8 Hz, CH_3); 3.04 (m, 1H, J = 6.8 Hz, CH); 3.94 (s, 2H, CH_2); 4.62 (s, 2H, CH_2COOH); 6.86 (d, 2H, J = 8.4 Hz, Ar); 7.12 (d, 3H, J = 8.8 Hz, Ar); 7.25 (d, 1H, J = 2.0, 8.0 Hz, Ar); 7.34 (s, 1H, Ar); 7.91 (s, 1H, COOH) ppm. ^{13}C NMR (CD_3OD-d_4): δ 171.44 (COOH); (157.82, 144.57, 143.37, 135.01, 130.83, 128.63, 128.60, 124.20, 115.67) Ar; 66.03 (CH_2COOH); 41.29 (CH_2); 28.64 (CH); 23.79 (CH_3) ppm. Anal. Calcd for $C_{18}H_{21}NO_3$: C, 72.22%; H, 7.07%; N, 4.68%. Found: C, 72.27%; H, 7.12%; N, 4.39%.

4.1.1.5. General procedure for synthesis of compounds 5, 6 and 8. Under nitrogen atmosphere, $AlCl_3$ (1.35 mmol) was added to a solution of $LiAlH_4$ (1.35 mmol) in THF. The mixture was stirred at rt for 5 min; then, a solution of the proper cyanoderivative **22**, **23** or **31** (0.15 mmol) in THF was added dropwise, and the mixture refluxed for 12 h. After cooling at 0 °C, the mixture was diluted with water, acidified with HCl 10% and washed with Et_2O. Aqueous phase was alkalinized with NaOH 1 N and extracted with chloroform; then, organic phase was filtered through Celite, washed with brine, dried over Na_2SO_4 and concentrated.

4.1.1.6. Synthesis of 4-(4-(2-aminoethoxy)-2,6-dimethylbenzyl)-N-ethyl-2-isopropylaniline (5). The crude product was transformed in the corresponding hydrochloride salt. Yield: 15% (grey powder) ^{1}H NMR (CD_3OD-d_4): δ 1.23 (d, 6H, J = 6.8 Hz, CH_3); 1.36 (t, 3H, J = 7.4 Hz, CH_2); 2.20 (s, 6H, CH_3); 3.02–3.06 (m, 1H, CH); 3.36–3.40 (m, 4H, CH_2NH_2, CH_2); 4.07 (s, 2H, CH_2); 4.22 (t, J = 4.8 Hz, 2H, OCH_2); 6.77 (s, 2H, Ar); 6.97 (dd, 1H, J = 1.4,8.0 Hz, Ar); 7.21 (d, 1H, J = 1.4 Hz, Ar); 7.27 (d, 1H, J = 8.0 Hz, Ar) ppm. ^{13}C NMR (CD_3OD-d_4): δ 157.89, 144.36, 143.49, 139.71, 130.74, 130.50, 128.61, 127.99, 124.54, 115.19, 65.06, 40.42, 34.67, 28.66, 24.46, 20.43, 20.36, 11.36 ppm. Anal. Calcd for $C_{22}H_{33}ClN_2O$: C, 70.10%; H, 8.82%; N, 7.43%; Found: C, 70.24%; H, 8.75%; N, 7.56%.

4.1.1.7. Synthesis of 4-(4-(2-aminoethoxy)-2-(trifluoromethyl) benzyl)-N-ethyl-2-isopropylaniline (6). The crude was purified by transformation in hydrochloric salt and subsequent recrystallization in isopropanol/diisopropyl ether. Yield: 17% (yellow oil). ^{1}H NMR (CD_3OD-d_4): δ 1.27 (d, J = 6.4 Hz, 6H, CH_3); 1.36 (t, J = 7.4 Hz, 3H, CH_3); 3.03–3.04 (m, 1H, CH); 3.38–3.41 (m, 4H, CH_2NH_2, CH_2); 4.19 (s, 2H, CH_2); 4.29 (t, 2H, J = 8.0 Hz, CH_2O); 7.11 (dd, J = 2.0, 8.4 Hz, 1H, Ar); 7.23 (dd, 2H, J = 2.4, 8.4 Hz, 1H, Ar); 7.28–7.37 (m, 4H, Ar) ppm. ^{13}C NMR (CD_3OD-d_4): δ 158.10, 143.52, 135.03, 134.77, 132.28, 131.02, 130.72, 129.55, 128.94, 124.40, 124.19, 119.09, 113.96, 65.76, 40.20, 37.67, 28.74, 24.41, 17.28, 11.42 ppm. Anal. Calcd for $C_{21}H_{28}ClF_3N_2O$: C, 60.50%; H, 6.77%; N, 6.72%; Found: C, 60.51%; H, 6.72%; N, 6.71%.

4.1.1.8. Synthesis of 4-(4-(2-aminoethoxy)-2,6-dimethylbenzyl) phenol (7). Aniline derivative **34** (0.17 mmol, 48 mg) was solubilized in water and treated with H_2SO_4 (0.05 mL). The mixture obtained was stirred for 20 min at 0 °C. Then, a solution of $NaNO_2$ (0.17 mmol; 12 mg) in H_2O was added and the reaction refluxed for 1 h. After this time, reaction mixture was cooled at RT and diluted with AcOEt. Organic phase was then washed with a saturated solution of NaCl, dried, filtered and concentrated. The crude obtained was purified by precipitation in MeOH/Et_2O. Yield 42% (dark yellow powder). ^{1}H NMR (CD_3OD-d_6): δ 2.19 (s, 6H, CH_3); 3.09 (t, J = 5.0 Hz; 2H, CH_2NH_2); 3.88 (s, 2H, CH_2); 3.99 (t, J = 5.0 Hz; 2H, OCH_2); 6.61 (s, 2H, Ar); 6.69 (d, J = 8.6, 2H, Ar); 6.83 (d, J = 8.6, 2H, Ar) ppm. ^{13}C NMR (CD_3OD-d_6): δ 158.24, 156.33, 139.34, 132.20, 131.26, 129.62, 116.09, 115.11, 69.76, 41.84, 34.21, 20.54 ppm. Anal. Calcd for $C_{17}H_{21}NO_2$: C, 75.25%; H, 7.80%; N, 5.16%; Found: C, 75.19%; H, 7.66%; N, 4.88%.

4.1.1.9. Synthesis of 4-(4-(2-aminoethoxy)-2-(trifluoromethyl) benzyl)aniline (8). The crude product was transformed in the corresponding hydrochloride salt. Yield: 10% (yellow oil). ^{1}H NMR (CD_3OD-d4): δ 3.39 (t, J = 4.8 Hz, 2H, CH_2NH_2); 4.19 (s, 2H, CH_2); 4.29 (t, J = 4.8 Hz, 2H, CH_2); 7.23 (dd, J = 2.4, 8.4 Hz, 1H Ar); 7.27–7.35 (m, 6H Ar) ppm. ^{13}C NMR (CD_3OD-d_4): δ 158.09, 143.25, 135.05, 132.29, 131.44, 130.89, 130.10, 126.97, 124.13, 119.10, 113.98, 65.78, 40.21, 37.53 ppm. Anal. Calcd for $C_{16}H_{17}F_3N_2O$: C, 61.93%; H, 5.52%; N, 9.03%; Found: C, 62.07%; H, 5.42%; N, 9.26%.

4.1.1.10. Synthesis of 2-(4-(4-aminobenzyl)-3-fluorophenoxy)acetic acid (9). A solution of derivative **35** (28 mg, 0.109 mmol) in H_2O was acidified with HCl 37% and refluxed at 100 °C for 4 h. Then the mixture was concentrated affording the crude **9**, which was purified by formation of the corresponding hydrochloride salt. Yield: 77% (grey powder). ^{1}H NMR (CD_3OD-d_4): δ 3.98 (s, 2H, CH_2); 4.66 (s, 2H, CH_2COOH); 6.69–6.74 (m, 2H, Ar); 7.15 (d, 1H, J = 8.4 Hz, Ar);

7.31–7.37 (m, 4H, Ar) ppm. ^{13}C NMR (CD_3OD-d_4): δ 172.21(COOH); [161.28, 159.50, 143.21, 132.57, 131,21, 129.81, 124.10, 121.30, 111.53, 103.49] Ar; 66.03 (CH_2COOH); 34.51 (CH_2) ppm. Anal. Calcd for $C_{15}H_{14}FNO_3$: C, 65.45%; H, 5.13%; N, 5.09%; Found: C, 65.27%; H, 5.18%; N, 5.21%.

4.1.1.11. Synthesis of 2-(4-(4-aminobenzyl)-3,5-dimethylphenoxy) acetic acid (10). Ester **36** (0.12 mmol; 39 mg) solubilized in MeOH was treated with an aqueous solution of NaOH 10% (0.02 mL). Mixture was then refluxed for 1h and then, concentrated in vacuo. The crude obtained was purified by precipitation in MeOH/Et_2O providing compound **10**. Yield: 42% (pale yellow). ^{1}H NMR (CD_3OD-d_4): δ 2.17 (s, 6H, CH_3); 3.85 (s, 2H, CH_2); 4.34 (s, 2H, CH_2COOH); 6.61 (d, 2H, $J = 8.4$ Hz, Ar); 6.65 (s, 2H, Ar); 6.72 (d, 2H, $J = 8.4$ Hz, Ar) ppm. ^{13}C NMR (CD_3OD-d_4): δ 177.01, 157.94, 146.00, 139.15, 131.39, 131.25, 129.36, 117.00, 115.25, 68.47, 34.27, 20.54 ppm. Anal. Calcd for $C_{17}H_{19}NO_3$: C, 71.56%; H, 6.71%; N, 4.91%; Found: C, 71.38%; H, 6.92%; N, 5.07%.

4.1.1.12. Synthesis of 2-(4-(4-hydroxybenzyl)-3,5-dimethylphenoxy) acetic acid (11). Aniline **10** (0.20 mmol; 64 mg) was dissolved in H_2O, added to a solution of H_2SO_4 at concentrated grade (0.05 mL), and left under stirring at 0 °C for 20 min. Then, a solution of $NaNO_2$ (0.20 mmol; 14 mg) in H_2O was added, and the mixture was refluxed for 1 h. After this time, the reaction was allowed to cold down to rt and then diluted with AcOEt. Organic phase was washed with a saturated solution of NaCl, then dried, filtered and evaporated. The crude product was purified by precipitation in AcOEt/Hexane. Yield: 35% (brown powder). ^{1}H NMR (CD_3OD-d_4): δ 2.17 (s, 6H, CH_3); 3.87 (s, 2H, CH_2); 4.59 (s, 2H, CH_2COOH); 6.60–6.67 (m, 4H, Ar); 6.77 (d, 2H, $J = 8.4$ Hz, Ar) ppm. ^{13}C NMR (CD_3OD-d_4): δ 173.18, 157.42, 156.32, 139.45, 132.10, 131.86, 129.64, 116.09, 115.12, 65.94, 34.21, 20.53 ppm. Anal. Calcd for $C_{17}H_{18}O_4$: C, 71.31%; H, 6.34%. Found: C, 71.46%; H, 6.47%.

4.1.2. X-ray selection

To date, many X-ray structures of TRα and TRβ in complex with T3, GC-1, KB131084 and other thyromimetics, are available in the Protein Data Bank (PDB). A superposition on the α-carbon atoms of all these structures, showed that the general protein folding is highly preserved, with a good conservation of both the secondary structure and the side chain orientation, especially within the LBC. Thus, among the crystals with highest resolution, those co-crystallized with our ligands progenitor GC-1 were chosen for our docking calculations: PDB codes 3ILZ and 3IMY, for TRα and TRβ, respectively.

4.1.3. Docking calculations

The ligands tridimensional structure were generated with the Maestro Build Panel and prepared using Ligprep predicting all tautomeric and protonation states at physiological pH (7.4 ± 1.5). The receptor structures were prepared using the Protein Preparation Wizard implemented in Maestro Suite (Schrödinger Release 2019–2: Schrödinger Suite 2019–1), deleting all water molecules with the exception of those within 3 Å from the ligand, adding missing hydrogen atoms and minimizing the complexes. The docking grid was calculated through the grid generation tool in Glide 6.7 [37–39] and centered around the crystallized ligand using default settings. The OPLS3E force field was employed for docking. The results of calculations were evaluated and ranked based on the Glide SP scoring function.

4.2. In vitro studies

4.2.1. Activity against thyroid hormone receptors

Assays on selected compounds were performed by SelectScreen™ Biochemical Nuclear Receptor Profiling Service (Thermofisher Scientific, US) using the LanthaScreenTM TR-FRET Nuclear Receptor Coregulator Assay (service provided by Invitrogen Corporation, USA), as reported on the company's website. (https://www.thermofisher.com/it/en/home/products-and-services/services/custom-services/screening-and-profiling-services/selectscreen-profiling-service/selectscreen-cell-based-nuclear-receptor-profiling-services.html).

4.2.2. Human hepatocellular carcinoma (HepG2) cell culture and treatment with compounds 1 and 3

The human hepatocellular carcinoma HepG2 cells line was purchased from the American Type Culture Collection (ATCC HB-8065, Rockville, MD, USA) and cultured in low glucose (LG) DMEM supplemented with 10% FBS, 100 IU/mL penicillin G sodium and 100 μg/mL streptomycin sulfate (Invitrogen, Paisley, UK) incubating in a humidified atmosphere with 5% CO_2 at 37 °C. These cells were then treated with 1 and 10 μM concentrations of test compounds for 24 h. After treatments, cells were lysed in a buffer containing 20 mM Tris–HCl (pH 7.5), 0.9% NaCl, 0.2% Triton X-100, and 1% of the protease inhibitor cocktail (Sigma-Aldrich, Milan, Italy) and then stored at −80 °C for further Western blot analysis. All the analyses were conducted on cells between the third and the sixth passage.

4.2.3. Oil red O (ORO) staining of lipid accumulation in HepG2 cells

Total lipid accumulation was evaluated according to the method previously described by Liu et al. [40] Cells were seeded at a density of 3.5 × 104 cells/well in 1 mL of lipogenic growth medium (HG-DMEM) and treated for 24 h with compound **1** or **3**, at 1 and 10 μM. Cloroquine (25 μM) was used as positive control. Subsequently, after collecting the growth media to be used to perform glycerol level measurements (as detailed below), cells were rinsed twice with PBS and fixed in 4% paraformaldehyde in PBS at 4 °C for 30 min. After 3 washes with cold PBS, cells were stained with ORO working solution, prepared as described above, for 30 min at room temperature and subsequently rinsed again with PBS.

4.2.4. Determination of glycerol release from HepG2 cells

After treatment with test compounds, cell culture supernatants were collected from each well and placed in glycerol-free containers. A 125 μg/mL Glycerol Standard Solution (Abcam, Milan, Italy) was used to make a #1 through #8 standard curve. 25 μL of each supernatant and standard were then transferred into a 96-well plate and 100 μL of either Free Glycerol Assay Reagent (Abcam, Milan, Italy) or MilliQ water added to each well. After incubation at rt for 15 min, glycerol levels were measured by reading absorbance at 540 nm (Bio-Rad 680, Milan, Italy).

4.2.5. Western Blotting analysis

Proteins (20–30 μg) were separated on CriterionTGX TM gel (4–20%) and transferred on Immuno-PVDF membrane (Biorad, Milan, Italy) for 30 min. The membranes were then incubated overnight at 4 °C with one of the following the specific primary antibodies: anti-p-AMPKα1-thr172, anti-AMPK, anti-p-ACC-ser79, anti-ACC (Cell Signaling Technology, Danvers, MA, USA). Then, blots were washed 3 times for 10 min with 1× TBS, 0.1% Tween®20 and incubated for 2 h with secondary antibody (peroxidase-coupled anti rabbit in 1× TBS, 0.1% Tween®20). After washing 3 times for 10 min, the reactive signals were revealed by an enhanced ECL Western Blotting analysis system (Amersham, Milan, Italy). Band

densitometric analysis was performed using Image Lab Software (Biorad, Milan, Italy).

4.2.6. In vivo studies

Five-week-old male F-344 rats purchased from Charles River (Milano, Italy) were maintained on a standard laboratory diet (Ditta Mucedola, Milano, Italy). The animals were given food and water ad libitum with a 12 h light/dark daily cycle and were acclimated for 1 week before the start of the experiment. All procedures were performed in accordance with the Guidelines for the Care and Use of Laboratory Animals and were approved by the Italian Ministry of Health. Animals were treated with daily intragastric (IG) injections for 3 days of **1** or **3** (50, 75 and 100 μg/100 g b. w) or T3 (20 μg/100 g b. wt). A control group received the vehicle (DMSO 5% in corn oil). Additional two groups received daily injections of either **1** or **3** at the dose of 75 μg/100 g b. wt. intraperitoneally for 3 days.

4.2.7. Analysis of serum aspartate aminotransferase (AST), alanine aminotransferase (ALT), triglycerides (TGs) and cholesterol (CH)

Immediately after sacrifice, blood samples were collected from the abdominal aorta, serum was separated by centrifugation (2000 g for 20 min) and tested for triglycerides, cholesterol, aspartate aminotransferase and alanine aminotransferase using a commercially available kit from Boehringer (Mannheim, Germany).

4.3. Statistical analysis

Statistical analyses were performed using GraphPad Prism version 6.0 for Windows (GraphPad Software, San Diego, CA, USA). Data were subjected to One-Way analysis of variance for mean comparison, and significant differences among different treatments were calculated according to Tukey's HSD (honest significant difference) multiple range test. Data are reported as mean ± SEM. Differences at $p < 0.05$ were considered statistically significant.

4.4. Associated content

The Supporting Information is available free of charge on the Elsevier website at DOI:

Author contributions

MR and SS carried out the synthesis. LB and GC carried out the experiments in HepG2 and adipocytes and analyzed the data. VLP, VMD and LM carried out the computational studies. AP, MAK and AC carried out the in vivo experiments and the data analysis. MR and SG carried out the off-target and ADME-Tox profiling assays and analyzed the data. SR and GC design and coordinate the project. All authors discussed the results and contributed to the final manuscript. MR, SR, AC and GC wrote the manuscript.

Funding sources

This work was supported by grants from International Society of Drug Discovery (ISDD) (Milan), from the University of Pisa [Progetti di Ricerca di Ateneo PRA_2017_55 (to GC) and PRA_2018_20 (to SR)], from Associazione Italiana Ricerca sul Cancro (AIRC, IG-20176 to AC) and from Regione Autonoma Sardegna (RAS to AC).

Declaration of competing interest

The authors declare that they have no known competing financial interests or personal relationships that could have appeared to influence the work reported in this paper.

Acknowledgment

We thank the COST action CA15135 (Multitarget Paradigm for Innovative Ligand Identification in the Drug Discovery Process MuTaLig) for support the working experience of MR at the Fraunhofer-IME DE (Hamburg, Germany). We also thank POR FSE 2014–2020 – Regione Toscana and the University of Pisa for financing the fellowship to SS and Fondazione Umberto Veronesi for financing to MAK the fellowship.

Appendix A. Supplementary data

Supplementary data to this article can be found online at https://doi.org/10.1016/j.ejmech.2019.112006.

Abbreviations

THs	thyroid hormones
TRα	thyroid hormone receptor α
TRβ	thyroid hormone receptor β
NAFLD	non-alcoholic fatty-liver disease

References

[1] P.M. Yen, Physiological and molecular basis of thyroid hormone action, Physiol. Rev. 81 (2001) 1097–1142.
[2] G.A. Brent, Mechanisms of thyroid hormone action, J. Clin. Investig. 122 (2012) 3035–3043.
[3] R. Kapoor, S.E. Fanibunda, L.A. Desouza, S.K. Guha, V.A. Vaidya, Perspectives on thyroid hormone action in adult neurogenesis, J. Neurochem. 133 (2015) 599–616.
[4] E.G. Baxi, J.T. Schott, A.N. Fairchild, L.A. Kirby, R. Karani, P. Uapinyoying, C. Pardo-Villamizar, J.R. Rothstein, D.E. Bergles, P.A. Calabresi, A selective thyroid hormone beta receptor agonist enhances human and rodent oligodendrocyte differentiation, Glia 62 (2014) 1513–1529.
[5] J.A. Vaitkus, J.S. Farrar, F.S. Celi, Thyroid hormone mediated modulation of energy expenditure, Int. J. Mol. Sci. 16 (2015) 16158–16175.
[6] I. Tancevski, P. Eller, J.R. Patsch, A. Ritsch, The resurgence of thyromimetics as lipid-modifying agents, Curr. Opin. Investig. Drugs 10 (2009) 912–918.
[7] H. Gullberg, M. Rudling, C. Salto, D. Forrest, B. Angelin, B. Vennstrom, Requirement for thyroid hormone receptor beta in T3 regulation of cholesterol metabolism in mice, Mol. Endocrinol. 16 (2002) 1767–1777.
[8] M.A. Kowalik, A. Columbano, A. Perra, Thyroid hormones, thyromimetics and their metabolites in the treatment of liver disease, Front. Endocrinol. 9 (2018) 382.
[9] G. Chiellini, J.W. Apriletti, H.A. Yoshihara, J.D. Baxter, R.C. Ribeiro, T.S. Scanlan, A high-affinity subtype-selective agonist ligand for the thyroid hormone receptor, Chem. Biol. 5 (1998) 299–306.
[10] M.D. Erion, E.E. Cable, B.R. Ito, H. Jiang, J.M. Fujitaki, P.D. Finn, B.H. Zhang, J. Hou, S.H. Boyer, P.D. van Poelje, D.L. Linemeyer, Targeting thyroid hormone receptor-beta agonists to the liver reduces cholesterol and triglycerides and improves the therapeutic index, Proc. Natl. Acad. Sci. U. S. A. 104 (2007) 15490–15495.
[11] A. Berkenstam, J. Kristensen, K. Mellstrom, B. Carlsson, J. Malm, S. Rehnmark, N. Garg, C.M. Andersson, M. Rudling, F. Sjoberg, B. Angelin, J.D. Baxter, The thyroid hormone mimetic compound KB2115 lowers plasma LDL cholesterol and stimulates bile acid synthesis without cardiac effects in humans, Proc. Natl. Acad. Sci. U. S. A. 105 (2008) 663–667.
[12] L. Johansson, M. Rudling, T.S. Scanlan, T. Lundasen, P. Webb, J. Baxter, B. Angelin, P. Parini, Selective thyroid receptor modulation by GC-1 reduces serum lipids and stimulates steps of reverse cholesterol transport in euthyroid mice, Proc. Natl. Acad. Sci. U. S. A. 102 (2005) 10297–10302.
[13] I. Tancevski, M. Rudling, P. Eller, Thyromimetics: a journey from bench to bedside, Pharmacol. Ther. 131 (2011) 33–39.
[14] S. Meruvu, S.D. Ayers, G. Winnier, P. Webb, Thyroid hormone analogues: where do we stand in 2013? Thyroid 23 (2013) 1333–1344.
[15] L.P. Elbers, J.J. Kastelein, B. Sjouke, Thyroid hormone mimetics: the past, current status and future challenges, Curr. Atheroscler. Rep. 18 (2016) 14.
[16] J. Zhou, L.R. Waskowicz, A. Lim, X.H. Liao, B. Lian, H. Masamune, S. Refetoff, B. Tran, D.D. Koeberl, P.M. Yen, A liver-specific thyromimetic, VK2809, decreases hepatosteatosis in glycogen storage disease type Ia, Thyroid 29 (2019) 1158–1167.
[17] G. Chiellini, G. Nesi, S. Sestito, S. Chiarugi, M. Runfola, S. Espinoza, M. Sabatini, L. Bellusci, A. Laurino, E. Cichero, R.R. Gainetdinov, P. Fossa, L. Raimondi, R. Zucchi, S. Rapposelli, Hit-to-Lead optimization of mouse trace amine associated receptor 1 (mTAAR1) agonists with a diphenylmethane-scaffold: design, synthesis, and biological study, J. Med. Chem. 59 (2016) 9825–9836.

[18] L. Bellusci, A. Laurino, M. Sabatini, S. Sestito, P. Lenzi, L. Raimondi, S. Rapposelli, F. Biagioni, F. Fornai, A. Salvetti, New insights into the potential roles of 3-iodothyronamine (T1AM) and newly developed thyronamine-like TAAR1 agonists in neuroprotection, Front. Pharmacol. 8 (2017) 905.
[19] H.A. Yoshihara, J.W. Apriletti, J.D. Baxter, T.S. Scanlan, Structural determinants of selective thyromimetics, J. Med. Chem. 46 (2003) 3152–3161.
[20] G. Chiellini, G. Nesi, M. Digiacomo, R. Malvasi, S. Espinoza, M. Sabatini, S. Frascarelli, A. Laurino, E. Cichero, M. Macchia, R.R. Gainetdinov, P. Fossa, L. Raimondi, R. Zucchi, S. Rapposelli, Design, synthesis, and evaluation of thyronamine analogues as novel potent mouse trace amine associated receptor 1 (mTAAR1) agonists, J. Med. Chem. 58 (2015) 5096–5107.
[21] W.E. Evans, M.V. Relling, Pharmacogenomics: translating functional genomics into rational therapeutics, Science 286 (1999) 487–491.
[22] I.L. Cote, S.D. McCullough, R.N. Hines, J.J. Vandenberg, Application of epigenetic data in human health risk assessment, Curr Opin Toxicol 6 (2017) 71–78.
[23] S. Gul, Epigenetic assays for chemical biology and drug discovery, Clin. Epigenet. 9 (2017) 41.
[24] S.W. Dietrich, M.B. Bolger, P.A. Kollman, E.C. Jorgensen, Thyroxine analogues. 23. Quantitative structure-activity correlation studies of in vivo and in vitro thyromimetic activities, J. Med. Chem. 20 (1977) 863–880.
[25] L. Bleicher, R. Aparicio, F.M. Nunes, L. Martinez, S.M. Gomes Dias, A.C. Figueira, M.A. Santos, W.H. Venturelli, R. da Silva, P.M. Donate, F.A. Neves, L.A. Simeoni, J.D. Baxter, P. Webb, M.S. Skaf, I. Polikarpov, Structural basis of GC-1 selectivity for thyroid hormone receptor isoforms, BMC Struct. Biol. 8 (2008) 8.
[26] L. Martínez, A.S. Nascimento, F.M. Nunes, K. Phillips, R. Aparicio, S.M.G. Dias, A.C.M. Figueira, J.H. Lin, P. Nguyen, J.W. Apriletti, Gaining ligand selectivity in thyroid hormone receptors via entropy, Proc. Natl. Acad. Sci. U. S. A. 106 (2009) 20717–20722.
[27] J.J. Hangeland, A.M. Doweyko, T. Dejneka, T.J. Friends, P. Devasthale, K. Mellstrom, J. Sandberg, M. Grynfarb, J.S. Sack, H. Einspahr, M. Farnegardh, B. Husman, J. Ljunggren, K. Koehler, C. Sheppard, J. Malm, D.E. Ryono, Thyroid receptor ligands. Part 2: thyromimetics with improved selectivity for the thyroid hormone receptor beta, Bioorg. Med. Chem. Lett 14 (2004) 3549–3553.
[28] Y.L. Li, C. Litten, K.F. Koehler, K. Mellstrom, N. Garg, A.M. Garcia Collazo, M. Farnegard, M. Grynfarb, B. Husman, J. Sandberg, J. Malm, Thyroid receptor ligands. Part 4: 4'-amido bioisosteric ligands selective for the thyroid hormone receptor beta, Bioorg. Med. Chem. Lett 16 (2006) 884–886.
[29] D.H. Ipsen, J. Lykkesfeldt, P. Tveden-Nyborg, Molecular mechanisms of hepatic lipid accumulation in non-alcoholic fatty liver disease, Cell. Mol. Life Sci. 75 (2018) 3313–3327.
[30] R. Singh, S. Kaushik, Y. Wang, Y. Xiang, I. Novak, M. Komatsu, K. Tanaka, A.M. Cuervo, M.J. Czaja, Autophagy regulates lipid metabolism, Nature 458 (2009) 1131–1135.
[31] R.A. Sinha, B.K. Singh, P.M. Yen, Direct effects of thyroid hormones on hepatic lipid metabolism, Nat. Rev. Endocrinol. 14 (2018) 259–269.
[32] H.C. Chi, C.Y. Tsai, M.M. Tsai, C.T. Yeh, K.H. Lin, Molecular functions and clinical impact of thyroid hormone-triggered autophagy in liver-related diseases, J. Biomed. Sci. 26 (2019) 24.
[33] M. Gasparrini, F. Giampieri, J.M. Alvarez Suarez, L. Mazzoni, Y.F.H. T, J.L. Quiles, P. Bullon, M. Battino, AMPK as a new attractive therapeutic target for disease prevention: the role of dietary compounds AMPK and disease prevention, Curr. Drug Targets 17 (2016) 865–889.
[34] S.J. Wakil, L.A. Abu-Elheiga, Fatty acid metabolism: target for metabolic syndrome, J. Lipid Res. 50 (Suppl) (2009) S138–S143.
[35] D. Zhang, W. Wang, X. Sun, D. Xu, C. Wang, Q. Zhang, H. Wang, W. Luo, Y. Chen, H. Chen, AMPK regulates autophagy by phosphorylating BECN1 at threonine 388, Autophagy 12 (2016) 1447–1459.
[36] I. Tamargo-Gomez, G. Marino, AMPK: regulation of metabolic dynamics in the context of autophagy, Int. J. Mol. Sci. 19 (2018).
[37] R.A. Friesner, R.B. Murphy, M.P. Repasky, L.L. Frye, J.R. Greenwood, T.A. Halgren, P.C. Sanschagrin, D.T. Mainz, Extra precision glide: docking and scoring incorporating a model of hydrophobic enclosure for protein-ligand complexes, J. Med. Chem. 49 (2006) 6177–6196.
[38] T.A. Halgren, R.B. Murphy, R.A. Friesner, H.S. Beard, L.L. Frye, W.T. Pollard, J.L. Banks, Glide: a new approach for rapid, accurate docking and scoring. 2. Enrichment factors in database screening, J. Med. Chem. 47 (2004) 1750–1759.
[39] R.A. Friesner, J.L. Banks, R.B. Murphy, T.A. Halgren, J.J. Klicic, D.T. Mainz, M.P. Repasky, E.H. Knoll, M. Shelley, J.K. Perry, D.E. Shaw, P. Francis, P.S. Shenkin, Glide: a new approach for rapid, accurate docking and scoring. 1. Method and assessment of docking accuracy, J. Med. Chem. 47 (2004) 1739–1749.
[40] T.F. Liu, V.T. Vachharajani, B.K. Yoza, C.E. McCall, NAD+-dependent sirtuin 1 and 6 proteins coordinate a switch from glucose to fatty acid oxidation during the acute inflammatory response, J. Biol. Chem. 287 (2012) 25758–25769.